

Adaptive spatial compounding for improving ultrasound images of the epidural space on human subjects

Denis Tran^a, King-Wei Hor^a, Allaudin Kamani^b, Vickie Lessoway^c and Robert N. Rohling^a

^aDepartment of ECE, University of British Columbia, 2332 Main Mall, Vancouver, Canada;

^bDepartment of Anesthesia, University of British Columbia, 4500 Oak Street, Vancouver, Canada;

^cDepartment of Ultrasound, BC Women's Hospital and Health Centre, 4500 Oak Street, Vancouver, Canada

ABSTRACT

Administering epidural anesthesia can be a difficult procedure, especially for inexperienced physicians. The use of ultrasound imaging can help by showing the location of the key surrounding structures: the ligamentum flavum and the lamina of the vertebrae. The anatomical depiction of the interface between ligamentum flavum and epidural space is currently limited by speckle and anisotropic reflection. Previous work on phantoms showed that adaptive spatial compounding with non-rigid registration can improve the depiction of these features. This paper describes the development of an updated compounding algorithm and results from a clinical study. Average-based compounding may obscure anisotropic reflectors that only appear at certain beam angles, so a new median-based compounding technique is developed. In order to reduce the computational cost of the registration process, a linear prediction algorithm is used to reduce the search space for registration. The algorithms are tested on 20 human subjects. Comparisons are made among the reference image plus combinations of different compounding methods, warping and linear prediction. The gradient of the bone surfaces, the Laplacian of the ligamentum flavum, and the SNR and CNR are used to quantitatively assess the visibility of the features in the processed images. The results show a significant improvement in quality when median-based compounding with warping is used to align the set of beam-steered images and combine them. The improvement of the features makes detection of the epidural space easier.

Keywords: Contrast, image processing, image quality/display, registration, spatial compounding

1. INTRODUCTION

1.1 Epidural anesthesia in obstetrics

Obstetric subjects may require the use of anesthesia to reduce the pain of labour or of a cesarean section. Anesthesia is injected into the epidural space as shown on Fig. 1 and a nerve block for the lower body is then provided. The epidural space is typically found at depths between 20-90mm¹. A failed epidural needle insertion procedure by which the needle perforates the dura mater can cause the subject to experience post-operative headaches, and, in more severe cases where the needle damages the spinal cord, paralysis or death².

Anesthesia needs to be injected in several different doses and at different times into the epidural space of the subject. Rather than performing a separate epidural needle insertion procedure for every dose, increasing the risks of failure, the anesthesiologist inserts a catheter in the epidural space and anesthesia can then be delivered at any time thereafter.

Depending on the form and angle of the spinous processes (Fig. 1) on each vertebra, the doctor has to choose the best needle angle and puncture point that maximizes the chance of reaching the epidural space without touching bone, and with the fewest number of attempts to minimize subject discomfort. In general, the epidural needle is inserted perpendicularly to the skin surface because the space between the spinous processes of vertebrae lumbar 2 and lumbar 3 (L2/L3), and lumbar 3 and lumbar 4 (L3/L4), are usually best accessed at angle 0°, i.e. perpendicular to skin, as seen in Fig. 1. The anesthesiologist then slowly inserts a saline-filled needle while applying continuous force on the plunger to obtain pressure feedback from the tissue around the needle tip. When the needle tip reaches the epidural space, which is a fluid-filled cavity, the saline fluid is easily injected and a loss of resistance is felt. The anesthesiologist then knows that the needle

Further author information: (Send correspondence to D.T.)

D.T.: E-mail: denist@ece.ubc.ca

Medical Imaging 2008: Ultrasonic Imaging and Signal Processing, edited by Stephen A. McAleavey, Jan D'hooge, Proc. of SPIE Vol. 6920, 692001, (2008) · 1605-7422/08/\$18 · doi: 10.1117/12.769216

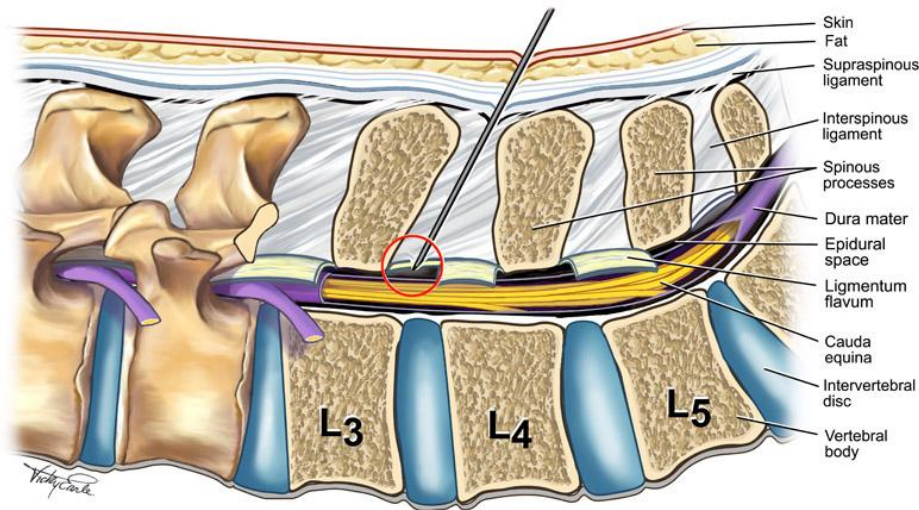


Figure 1. Epidural needle insertion, midline approach. The epidural space is circled.

tip has reached the epidural space. The catheter is then inserted through the epidural needle shaft into the epidural space. Next, the needle is removed leaving the catheter in place and anesthesia can finally be delivered at will via the catheter.

It has been observed that the use of ultrasound (US) to view the subject's lumbar anatomy facilitates the localization of the epidural space³ permitting an initial guess of the skin to epidural space depth. Moreover, it is suggested that ultrasound images can be used to get a-priori estimates of a suitable puncture point and needle insertion angle⁴ and this greatly improves the learning curve of inexperienced physicians and failures happen less frequently. A previous study⁵ showed two groups of residents performing epidural anesthesia, one with the help of ultrasound (ultrasound group) and the other without (control group). The ultrasound group achieved a success rate of 84% in the first 10 attempts whereas the control group had a success rate of 60%. Moreover, in the next 50 attempts, the ultrasound group achieved a success rate of 94% whereas the control group had a success rate of 86%. Epidural anesthesia is even more difficult when the subject has abnormal anatomical conditions such as scoliosis¹ and obesity. Ultrasonography was also used as real-time feedback for epidural procedures on young infants⁶, using the image instead of the traditional loss-of-resistance technique to detect the epidural space and the study shows a reduced number of bone contacts and an increase in the successful intraoperative analgesia rate from 90.5% to 100%. Although the study focuses on epidural depths of two month-old infants, which is around 7mm and much smaller than the epidural depth of adults (20-90mm), it shows the potential benefit of using ultrasound to visualize the lumbar region during an epidural needle insertion procedure.

1.2 Ultrasound imaging of lumbar region

Ultrasound is noninvasive, harmless at low power, portable, accurate and cost effective. However, ultrasound of the lumbar region shows an image filled with speckle and artifacts which can impede detection of important features such as the ligamentum flavum and other hard to detect structures. Ultrasound uses the pulse-echo technique to generate images. The received echo is based on ultrasound reflections from large-scale (relative to wavelength) structures, such as bone (i.e. specular reflection) and reflections from small-scale structures, such as cells (i.e. random scattering). However, if the specular reflection is strong enough, such as a bone, it casts shadows in the beam direction and structures underneath are obstructed. Random scattering creates speckle from constructive and destructive interference⁷. Although the texture of the speckle can be related to tissue type⁸, in general it is considered as a noise present throughout the image. Other artifacts such as reverberation and refraction also affect image quality. As the epidural space is a void, its location is estimated from more visible surrounding structures such as the ligamentum flavum, dura mater and laminae, plus prior knowledge of the lumbar anatomy.

Ultrasound reflects best when the wavefront encounters a structure perpendicular to the direction of propagation. In other words, since the ultrasound beam direction can be controlled, the propagation direction can be varied to some extent

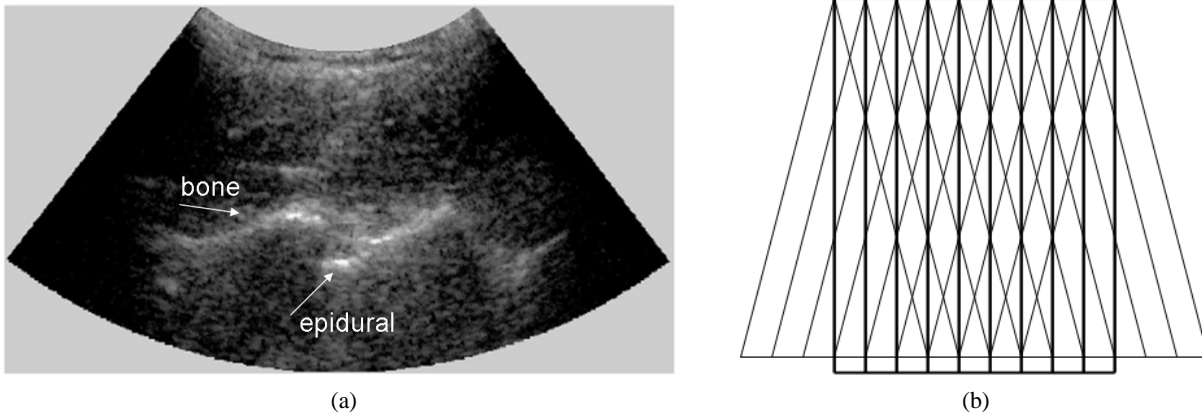


Figure 2. a) Ultrasound image of the lumbar spine with speckle noise and shadowing. A sagittal paramedian plane is used. b) Outlines of the reference and two beam steered images are shown. Spatial compounding uses positive and negative isonation angles to produce a set of beam-steered images that are subsequently combined.

with respect to the reflectors. If the angle at which the beam is steered is far from perpendicular to the surface of the structure, the structure may not appear clearly⁹. Some of these limitations are shown in Fig. 2(a).

1.3 Image processing techniques

Many post-processing methods employ filters to reduce speckle. Examples are the diffusion filter¹⁰, the adaptive weighted median filter¹¹, homogeneous region growing mean filter, and aggressive region growing filter¹². They all suffer to some degree from loss of fine detail resolution because of the removal of some high frequency content.

Compounding has been used previously in three ways to reduce speckle: temporal compounding, spatial compounding^{13 14 15} and frequency compounding¹⁶. The amount of speckle reduction, according to the theory of compounding, on the signal-to-noise ratio (SNR)¹⁷ can be as high as \sqrt{n} , where n is the number of images averaged.

Temporal compounding consists of averaging several images with either a slight movement of the tissues or of the transducer. This inherently introduces misalignment. Frequency compounding captures several images at the same location at different transmission frequencies, decorrelating the speckle patterns among images. Previous studies have shown modest improvements.

Spatial compounding is now popular among commercial manufacturers and will be presented in the next section. Wilhelm et al.¹⁸ studied various spatial compounding strategies with different parameters and found the average-based compounding to yield highest SNR and contrast. However, spatial compounding was performed on unregistered images where small misalignments tend to blur edges. A new median-based compounding will be presented in this work combined with non-rigid registration for feature alignment. stuff

2. SPATIAL COMPOUNDING WITH WARPING, LINEAR PREDICTION AND MEDIAN-BASED COMPOUNDING

2.1 Spatial compounding

Spatial compounding uses beam steering^{19 20 21}, which captures several frames by sending the ultrasound pulses at different angles of incidence (see Fig. 2(b) for an illustration of the principle). Since speckle noise is dependent on the distribution of small-scale reflectors along the ultrasound path²², changing the beam angle will also change the speckle noise pattern. Thus, the images will depict different noise patterns but similar anatomical features, so averaging these images should reduce the noise and features should be enhanced. Spatial compounding has been previously investigated as a way to improve other diagnostic tasks such as detecting atherosclerotic plaques^{14 15} and breast cancer²³. The application of spatial compounding to these images reduced speckle noise and improved the boundary continuity.

Spatial compounding also has other benefits, such as the possibility of enhancing structures that are only visible at certain beam angles. For example, certain weak but important features, such as a biopsy needle^{9 24} only appear at certain

beam angles because the surface of the weak feature is at an oblique angle to the ultrasound. The structure of main interest in this work is the epidural space, which is immediately under the ligamentum flavum and initial experience suggests it is only clear at certain beam angles.

2.2 Registration techniques

Despite the ability to rapidly steer the ultrasound beam and acquire several images in succession of the same region, conventional spatial compounding still suffers from blurring due to misalignment of features. The speed of sound varies by as much as 14% in soft tissue²⁵ and the resulting distortion (including refraction) causes the apparent positions of structures to be slightly different under different angles of incidence. Re-alignment of the features using an additional block-matching non-rigid registration (warping) was previously proposed by our group to properly align the structures of each image¹³. The result was a sharper ultrasound image. This method was tested on artificial phantoms, on a human forearm¹³ and recently on a spine phantom²⁶. Building on those results, the warping/compounding method is extended here to improve visibility of the ligamentum flavum in vivo, and therefore the epidural space.

2.2.1 Similarity measures

Registration performance is highly dependent on the similarity measure used as a cost function for finding the best alignment. A good similarity measure will yield a single strong peak upon best alignment.

Previous literature used several methods such as sum of absolute differences (SAD), mean squared error (MSE)²⁷, normalized covariance (NCOV), normalized crosscorrelation (NCC), entropy of the difference image and mutual information²⁸. Mutual information^{29 30} is a very popular similarity measure for registration of multimodality images but is too easily affected by artifacts. NCC and NCOV are very similar measures. Since the two images to be registered are quite similar, the means are assumed to be small enough so that the NCC and NCOV will yield similar results. The NCC is used for this work.

2.2.2 Interpolation and mapping

The beam-steered images are divided into blocks and each block registered to the reference image. Once the individual warping vectors have been found for each block, each pixel is assigned a warping vector by smooth interpolation.

Many interpolation techniques are well known and have been compared on operations such as resizing and rotation^{31 32 33}. Popular interpolation techniques are placed in order of performance as follows: nearest neighbour, linear, cubic and cubic B-spline. When testing the different methods, we found that performance was very similar so cubic interpolation was chosen since the computational cost is low.

Inverse mapping associates a vector to each pixel in the destination image, corresponding to a pixel in the original image. Inverse mapping does not encounter the problem of holes and overlapping like in forward mapping as each pixel has only one associated value. Inverse mapping is used here.

2.3 Linear prediction techniques

In order to further reduce computational cost, a coarse to fine or multi-resolution approach is often used where lower resolution blocks are registered and then higher resolution blocks are registered using a smaller search region¹³. This method, however does not make use of the trends in the warping vectors of neighbouring blocks.

Linear prediction³⁴ is a standard technique in audio coding in which one would give an initial guess of the current value based on a function of the previous values. The error signal, typically much smaller than the signal itself, requires fewer bits to be coded. The same idea can be used in making an initial guess at the value of the warping vector of the current block based on surrounding blocks, under the assumption that the warping vector field is smoothly varying. The search region for the current block can then be reduced.

This method starts at a location in the image with strong feature content to get reliable registration. The neighbouring blocks are then initialized with the value of the current block's warping vector, allowing a much smaller search region. This is repeated for all blocks in the image. The Canny edge detector is used for the purpose of detecting and counting edges and thus assess if a block is suitable for being the starting point for the linear prediction. The Canny edge detection technique³⁵ is a gradient-based method and is currently the most commonly used method^{36 37 38 39}.

When using linear prediction, one needs to define the first block for which one will find the warping vector, and the other blocks will follow. There are three sensible block positions to start. The first position is at the top of the image, where the refraction errors are smallest, therefore expecting the smallest warping required. However, the top of the image is often noisy with poor resolution so it is not suitable as the basis for finding the initial warping vectors. A second candidate is at the middle of the image, where a user is most likely to put the anatomical region of interest, and where the resolution is highest. However, it is not guaranteed to be the location with strong feature content and may contain shadows. The last location is where there are most edges (features). In this case, the Canny edge detector is used to detect areas containing edges, and then the block with the highest count is assumed to be the best starting candidate. This is a suitable choice for the first warping vector as it should produce the most accurate registration result. For shorter notation, we use LP2+ to designate linear prediction with a reduction of the search region by factor 2 in each direction using Canny to choose the initial block.

2.4 Median-based compounding

Since the features of interest do not appear on all frames, taking the average may not highlight weak anisotropic reflectors. Therefore, a new adaptive method is developed.

A gradient-based compounding method assumes a frame has a high information content at a given pixel when the image gradient is large at that location. Accordingly, any edges are weighted more than homogeneous regions. Many gradient calculation methods can be used. To avoid a response from relatively small-scale speckle noise, the gradient of a smoothed image is calculated using the Laplacian of a Gaussian (LoG). The key parameter is the size of the filter. This parameter should be set according to each type of image since speckle scale depends on probe characteristics such as frequency and depth setting. This method gives

$$p_{\text{gradient}}(x,y) = \frac{\sum_i^I G_i(x,y)p_i(x,y)}{\sum_i^I G_i(x,y)} \quad (1)$$

where $p_i(x,y)$, $G_i(x,y)$ are the pixel value, gradient of the image i at position (x,y) . $p_{\text{gradient}}(x,y)$ is the gradient-weighted average of all images at location (x,y) . Equation 1 calculates a weighted average of the pixels in different images, depending on their gradient. Since the specific goal of this new compounding method is to highlight weak reflectors near the epidural space, a nonlinear median operator may be more appropriate to generate a more distinct transition from light to dark regions. A median-based approach can be built upon the gradient calculations as follows:

$$P(x,y) = \{p_i(x,y) | G_i(x,y) > G_{\text{threshold}}, \forall i \in I\} \quad (2)$$

$$p_{\text{median}}(x,y) = \begin{cases} \text{median}(P(x,y)), & |P(x,y)| \geq \frac{|I|}{2} \\ p_{\text{gradient}}(x,y), & \text{otherwise} \end{cases} \quad (3)$$

where $P(x,y)$ is the set of all pixels $p_i(x,y)$ which have a $G_i(x,y)$ that is larger than a set threshold. $p_{\text{median}}(x,y)$ is the adaptive median of location (x,y) , meaning the median of all points in $P(x,y)$ if $P(x,y)$ contains more than half of the number of images, otherwise, it is $p_{\text{gradient}}(x,y)$. The median-based method builds on the gradient-based method with an added decision-making component: if a pixel combines mainly data with high feature content, the median of those points is used, otherwise, the gradient-based technique is used. In this way, the pixel retains a sharper response as it is no longer a weighted average, and speckle averaging of homogenous regions is retained.

2.5 Finding the right parameters

It is crucial to find the right parameters for the algorithm to yield best performance at a reasonable computational cost. The first choice is the number of beam-steered images and the number of degrees between each image. Too small an angle between each image and the speckle noise pattern will be highly correlated; too large and there will be few images within the range of angles that provide good image quality. We chose images from -8° to 8° with a step size of 2° as a good tradeoff between individual image quality and the number of images to average¹³.

2.5.1 Warping parameters

The second parameter to choose is the size of the blocks. The blocks must be large enough so that a block contains significant anatomical features, therefore making the registration more accurate, and small enough to produce a different warping vector for each block as each block is associated with a different refraction error.

The third parameter to choose is the size of the search region for aligning the blocks. A large region increases the chance of having high computational cost and misregistration, where a structure in the beam-steered image is matched with the wrong structure in the reference image. However, a small search region size means that the best registration may not be found.

Parameter selection was performed on a few sample images. Quantitative measures are computed on the regions of interest in each image and the parameters giving the best results are chosen. Table 1 shows the maximum Laplacian at the ligamentum flavum as the measure of interest. The search region is thus set to $\pm 8 \times \pm 2$ and the block size is set to 51 x 51 pixels.

Table 1. Maximum Laplacian of a slice at ligamentum flavum for a human subject in set 1 (this analysis should be done for each set of ultrasound transducer parameters)

hor x vert	block size						
	193	96	64	51	39	31	26
4x2	123	114	103	101	96	87	83
4x4	110	102	117	106	98	98	85
8x2	118	112	125	139	122	126	99
8x4	126	112	108	136	99	120	93

3. RESULTS AND DISCUSSION

3.1 Experimental setting

This study was approved by the Ethical Review Boards of the University of British Columbia and British Columbia Children's and Women's Health Centre and written informed consent was obtained from all subjects. Pregnant women at term in active labour or scheduled for elective cesarean section were included (n=20). Subjects who had contraindications to neuraxial anesthesia or who could not communicate in English were excluded. Subject biometrics were age 35 ± 4 years, weight 76 ± 15 kg, height 161 ± 7 and skin-to-epidural depth of 51 ± 11 mm.

Prior to epidural catheter placement, subjects were scanned using a 1-5MHz (centered at 3.3MHz) curvilinear probe (Ultrasonix Corp., Richmond, BC, Canada) in the paramedian plane. Images were recorded and the interspace between L3/L4 (lumbar vertebra 3 and lumbar vertebra 4) or L2/L3 interspace was reliably identified by using 'counting down' and 'counting up' techniques. Each subject was scanned in the sitting position with L3/L4 or L2/L3 interspaces identified using surface landmarks and confirmed by ultrasound. Images were taken with ultrasound depths between 0-60mm to 0-120mm. Pre-scan converted B-mode images showing the ligamentum flavum and laminae were captured over the range of beam steering angles. Examples scans are shown in Fig.3. The sonographer finds the best image and then the beam-steered frames are acquired.

3.2 Qualitative evaluation

We now compare the images before and after compounding with different compounding methods. Simple compounding (Fig. 4(b) and 5(b)) averages out most speckle, however, the ligamentum flavum and the bone boundaries are blurred. The doublet has been blurred to the point that it appears as one line. Using warping (Fig. 4(c) and 5(c)) sharpens the compounded image and the ligamentum flavum is seen as a doublet again. Using linear prediction (Fig. 4(d) and 5(d)) yields results that are faster but comparable to warping alone; the ligamentum flavum is still seen as a clear doublet. When using the median-based compounding (Fig. 4(e),4(f), 5(e),5(f)), the images are slightly sharper and more tissue details appear. Fig. 5 shows a case where the doublet is a very faint structure, compounding indeed loses the depiction of the doublet by blurring. The doublet starts to resurface after warping is used. And finally, the doublet appears clearer when using median-based spatial compounding with warping. When using LP2+ (Fig. 4(f), 4(f), 5(f), 5(f)), the depiction of the doublet is still clear, showing that quality does not degrade much when using LP2+ to reduce the computational cost.

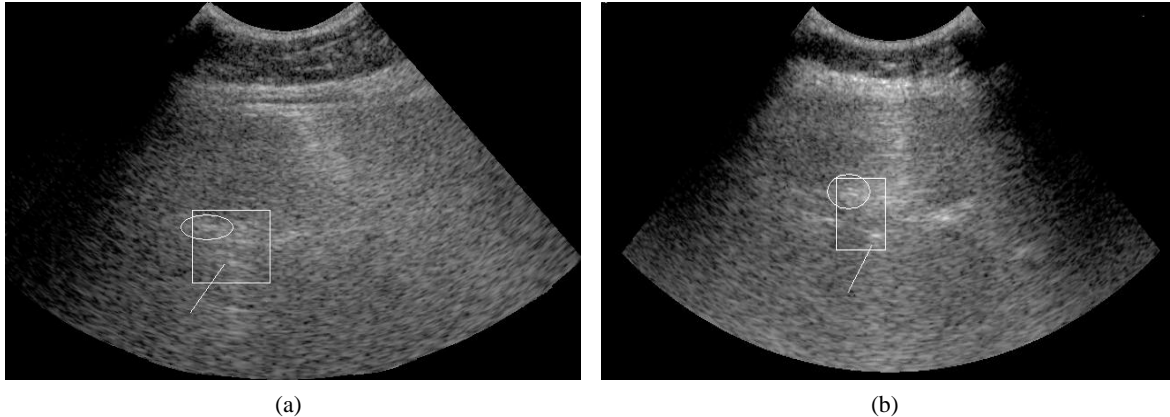


Figure 3. Images for subject 15 and 5; the region in the white rectangle is used for quantitative evaluation of features near the epidural space, the structure being pointed to is the ligamentum flavum doublet and the circled structure is the lamina or bone boundary.

3.3 Quantitative measures

There are two structures of interest in this clinical application: the ligamentum flavum and the lamina which is the bone seen in the images. For detecting bone boundaries, we would ideally have a sharp edge and therefore the gradient of the bone boundaries is taken as the quantitative measure. The ligamentum flavum is seen most of the time as a doublet. Ideally, we would see a set of sharp lines, therefore the Laplacian of the leading line is taken as the quantitative measure. The Laplacian is calculated by taking the gradient of the gradient. Since the features of interest are horizontal structures, the quantitative measures are computed on vertical line profiles through the image at the locations of interest.

The quantitative measures are calculated on all 20 sets of images and results are compiled in Table 2. Although the reference image scores highly, the features are difficult to discern due to speckle, as shown in Figs. 4(a) and 5(a).

Table 2. Gradient and Laplacian at regions of interest for human subjects for several methods

method	Laplacian of lig. flav.	gradient of bone boundaries
reference image	211 ± 59	59 ± 14
simple spatial compounding	132 ± 39	45 ± 16
average-based compounding with warping	148 ± 40	47 ± 16
median-based comp. w/ warping	163 ± 38	51 ± 17
average-based comp. w/ warping with LP2+	163 ± 44	50 ± 14
median-based comp. w/ warping with LP2+	155 ± 35	51 ± 16

Another important quantitative measure is speckle reduction. This can be measured through the computation of the signal-to-noise ratio (SNR) separately for light and dark regions, as well as the contrast-to-noise ratio (CNR), shown in Table 3. Here the compounding methods show a large improvement.

Table 3. SNR for light and dark regions and CNR

method	SNR light	SNR dark	CNR
reference image	6.0 ± 1.0	4.5 ± 1.5	1.9 ± 0.5
simple compounding	7.4 ± 1.6	7.5 ± 2.8	2.4 ± 0.7
average-based compounding with warping	7.2 ± 1.5	7.4 ± 2.8	2.4 ± 0.7
median-based comp. w/ warping	7.0 ± 1.4	6.8 ± 2.5	2.3 ± 0.6
average-based comp. w/ warping with LP2+	7.3 ± 1.8	7.3 ± 2.7	2.3 ± 0.8
median-based comp. w/ warping with LP2+	7.1 ± 1.7	6.6 ± 2.4	2.3 ± 0.8

3.4 Computational cost

The different methods presented above have various individual computational costs which are summarized in Table 4. Spatial compounding alone adds very little extra cost. Standard warping is very costly (479ms), and brings the maximum

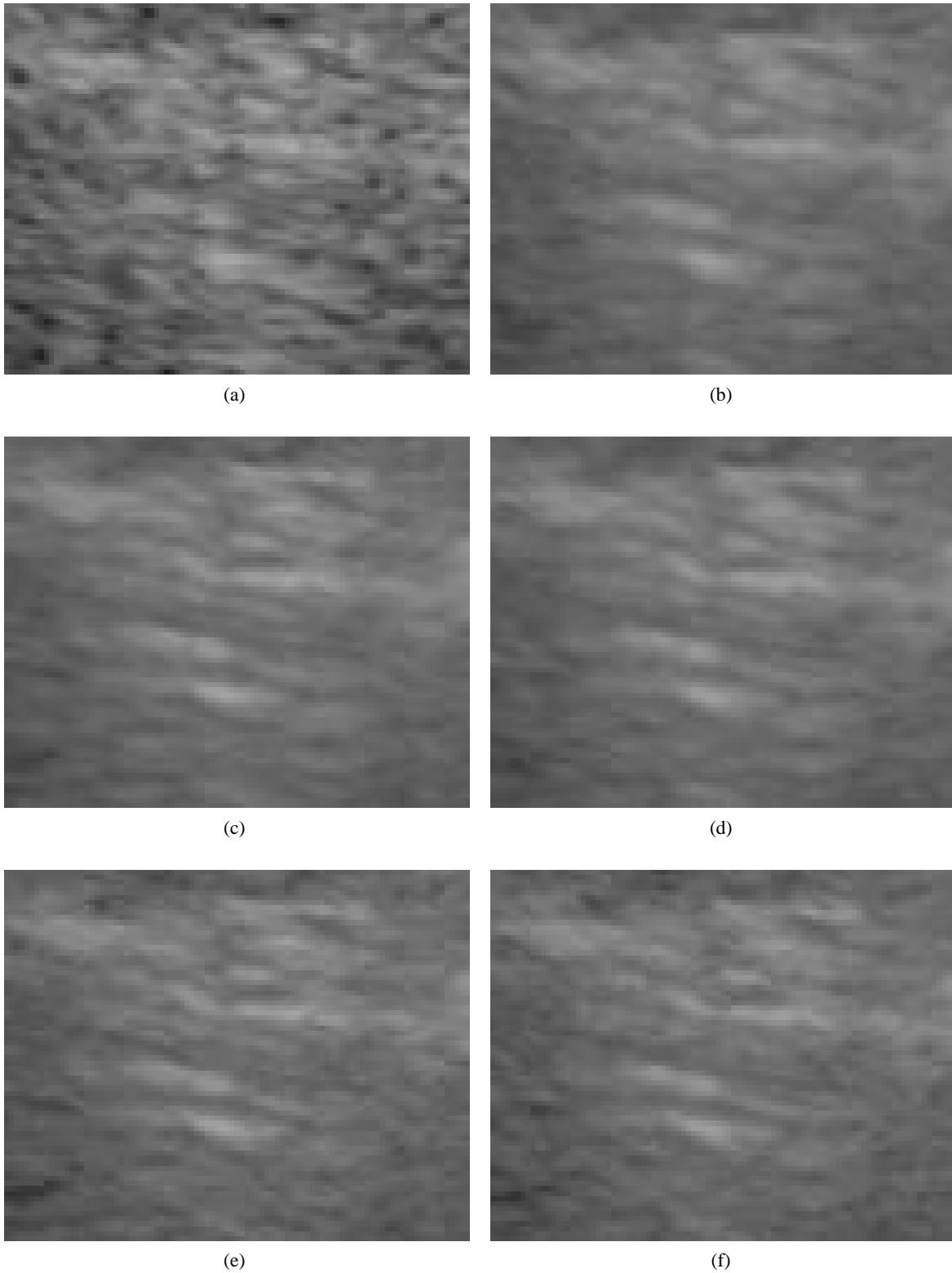


Figure 4. Images for subject 15 after compounding. The epidural space is the short horizontal line-pair near the middle. a) reference image, b) simple compounding, c) compounding with warping, d) compounding with warping and LP2+, e) median-based compounding with warping, f) median-based compounding with warping and LP2+.

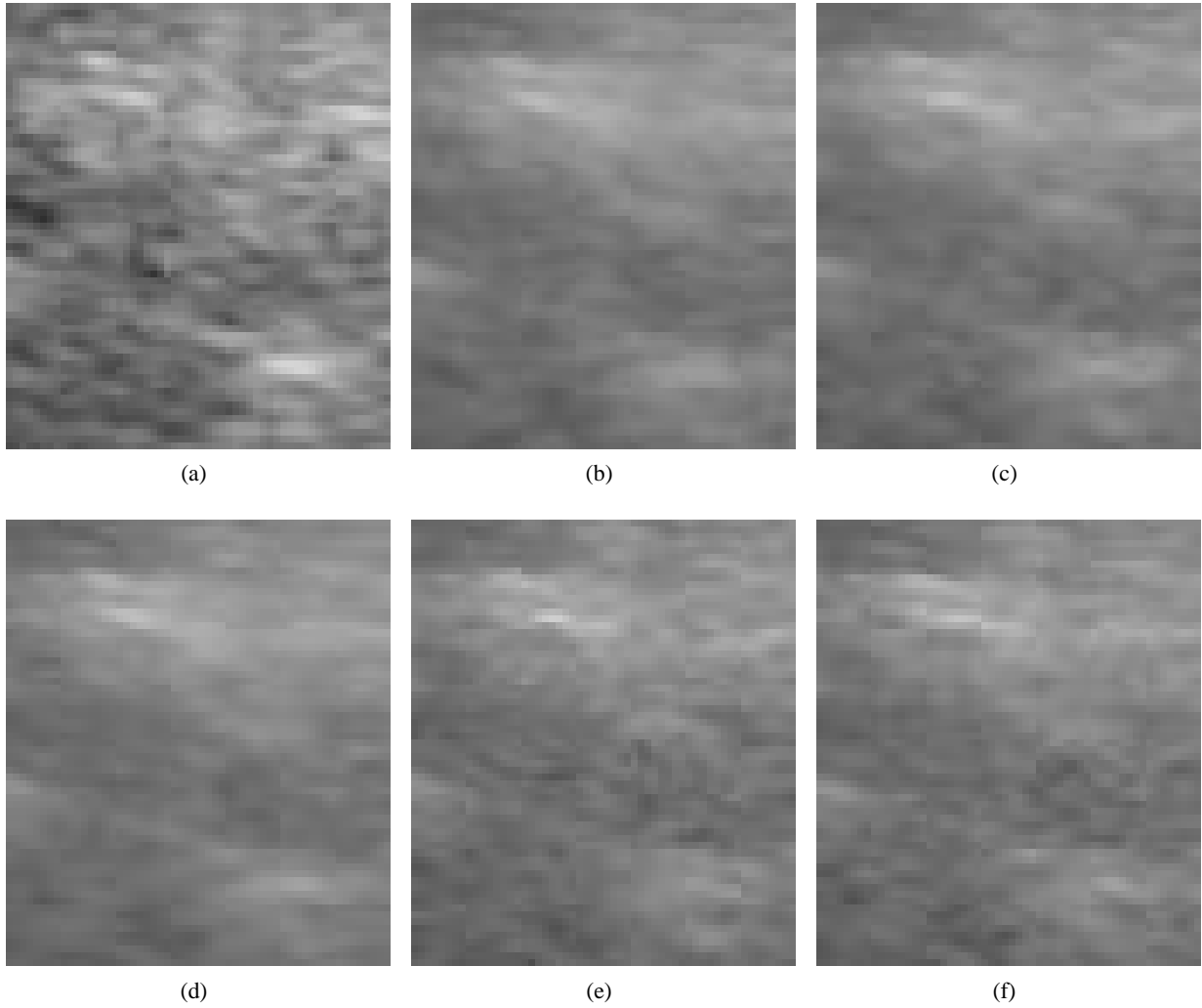


Figure 5. Images for subject 17 after compounding. The epidural space is the short horizontal line-pair at the bottom-left. a) reference image, b) simple compounding, c) compounding with warping, d) compounding with warping and LP2+, e) median-based compounding with warping, f) median-based compounding with warping and LP2+.

frame rate down to two frames per second which makes it impractical for real-time implementation. By using linear prediction to reduce the size of the search region by factor 2 in each direction (LP2+), the cost of finding the warping vectors becomes much smaller (130ms), but we must perform a Canny edge detection which costs 11ms. The median-based compounding takes 905ms, but more work can be done to reduce the cost of the median ⁴⁰.

Table 4. Computational cost of spatial compounding with warping for different parts of the algorithm. CPU time is calculated using a P4 3.0GHz with 1GB RAM, and a warping search region of $\pm 4 \times \pm 4$ (set 2 with image size 636 x 359) and $\pm 8 \times \pm 2$ (set 1 with image size 726 x 423) pixels.

method	image size		
	192x304	636 x 359	726 x 423
image resizing and angle correction	1.8	3.8	5.0
averaging images	4.2	10.7	14.3
displaying image	negligible	negligible	negligible
interpolating warping vectors	1.6	6.3	8.5
remapping the image	1.3	4.1	5.2
Canny edge detection	1.8	7.3	11.2
finding the warping vectors	94.6	354.4	479.8
finding the warping vectors with LP2+	27.4	96.7	130.3
adaptive median	164.6	662.2	904.9

4. DISCUSSION AND CONCLUSION

4.1 Summary

In many cases, it is very hard to look at an ultrasound image and find the ligamentum flavum. One usually relies on the lamina which is a stronger reflector to predict where the ligamentum flavum is. The images are heavily affected by speckle noise. When spatial compounding is used, it is more obvious where the features are but the features are blurred. Using warping makes edges clearer and thus makes the skin-to-epidural depth easier to measure. The choice of parameters will not only affect the intelligibility of the compounded image but also affects the computational cost. For each set of images, a set of parameters was found to yield the best compounded images for a reasonable cost. The test on 20 sets of human subjects show that real-time compounding with warping using an exhaustive search to align blocks of angled images to the reference frames yields a significant improvement to image quality and sharpness but is still not feasible on a standard processor. By using linear prediction, one can reduce the search region while maintaining good performance on reducing speckle noise and restoring continuous sharp boundaries on features such as bones and the ligamentum flavum. The median-based compounding yields sharper edges and certain details on surrounding tissues can be resolved but at a very high cost. The cost may be possible to reduce by using more sophisticated image combination algorithms.

4.2 Future work

With better ultrasound images of the lumbar region permitting an easier depiction of the ligamentum flavum, the next step would be to develop a system that can identify the ligamentum flavum and surrounding structures automatically, making the interpretation of ultrasound images even more obvious to the untrained anesthesiologist.

As 3D imaging becomes more useful and popular, spatial compounding will be extended to 3D, permitting arbitrary reslicing through the volume and perhaps a better depiction of the ligamentum flavum and surrounding structures. Computational costs will become a major issue when it comes to imaging. Complexity is roughly of the order n^2 in 2D and of the order n^3 for 3D. Efforts will be made to decrease computational complexity, following the techniques used to reduce computational complexity in the 2D case. For instance, linear prediction, with a gain factor of 4 in the 2D case theoretically decreases the cost by a factor 16, and in the 3D case the theoretical decrease is 64.

ACKNOWLEDGMENTS

This work is supported by a collaborative Health Research Project grant funded by the Natural Sciences and Engineering Research Council and the Canadian Institute of Health Research. Figure 1 was created by Vicky Earle of the Media Group at the University of British Columbia.

REFERENCES

1. T. Grau, R. W. Leipold, R. Conradi, and E. Martin, "Ultrasound control for presumed difficult epidural puncture," *Acta Anaesthesiol Scand* **45**, 766–771, 2001.
2. T. Grau, R. W. Leipold, S. Fatehi, E. Martin, and J. Motsch, "Real-time ultrasonic observation of combined spinal-epidural anaesthesia," *Eur J Anaesthesiol* **21**, 25–31, 2004.
3. T. Grau, R. W. Leipold, R. Conradi, E. Martin, and J. Motsch, "Ultrasound imaging facilitates localization of the epidural space during combined spinal and epidural anesthesia," *Reg Anesth Pain Med* **26**, 64–67, 2004.
4. C. Cristian Arzola, S. Davies, A. Rofaeel, and J. Carvalho, "Ultrasound using the transverse approach to the lumbar spine provides reliable landmarks for labor epidurals," *Anesthesia and Analgesia* **104**, 1188–1192, 2007.
5. T. Grau, E. Bartussek, R. Conradi, E. Martin, and J. Motsch, "Ultrasound imaging improves learning curves in obstetric epidural anesthesia: a preliminary study," *Can J Anaesth* **50**, 1047–1050, 2003.
6. H. Willschke, P. Marhofer, A. Bösenberg, S. Johnston, O. Wanzel, C. Sitzwohl, S. Kettner, and S. Kapral, "Epidural catheter placement in children: comparing a novel approach using ultrasound guidance and a standard loss-of-resistance technique," *British Journal of Anaesthesia* **97**, 200–207, 2006.
7. O. V. Michailovich and A. Tannenbaum, "Despeckling of medical ultrasound images," *IEEE Trans. on Ultrasonics, Ferroelectrics, and Frequency Control* **53**, 64–78, 2006.
8. S. Aja-Fernandez, M. Martin-Fernandez, and C. Alberola-Lopez, "Tissue identification in ultrasound images using rayleigh local parameter estimation," *Proceedings of the 7th IEEE International Conference on Bioinformatics and Bioengineering*, 1129–1133, 2007.
9. S. Cheung and R. Rohling, "Enhancement of needle visibility in ultrasound guided percutaneous procedures," *Ultrasound Med. Biol.* **30**, 617–624, 2004.
10. P. Perona and J. Malik, "Scale space and edge detection using anisotropic diffusion," *IEEE Trans. Pattern and Anal. Machine Intell.* **12**, 629–639, 1990.
11. T. Loupas, W. N. McDicken, and P. L. Allan, "An adaptive weighted median filter for speckle suppression in medical ultrasound images," *IEEE Trans. Circuits Syst.* **36**, 129–135, 1989.
12. Y. Chen, R. Yin, P. Flynn, and S. Broschat, "Aggressive region growing for speckle reduction in ultrasound images," *Pattern Recognition* **24**, 677–691, 2003.
13. A. Groves and R. Rohling, "Two dimensional spatial compounding with warping," *Ultrasound Med. Biol.* **30**, 929–942, 2004.
14. S. Huber, M. Wagner, M. Medl, and H. Czerbirek, "Real-time spatial compound imaging in breast ultrasound," *Ultrasound Med. Biol.* **28**, 155–163, 2002.
15. S. K. Jespersen, J. E. Wilhjelm, and H. Sillesen, "In vitro spatial compound scanning for improved visualization of atherosclerosis," *Ultrasound Med. Biol.* **26**, 1357–1362, 2000.
16. G. E. Trahey, S. W. Allison, J.W. and Smith, and O. T. Von Ramm, "A quantitative approach to speckle reduction via frequency compounding," *Ultrasonic Imaging* **8**, 151–164, 1986.
17. R. C. Gonzales and R. E. Woods, *Digital image processing*, Prentice Hall, 2 ed., 2000.
18. J. E. Wilhjelm, M. S. Jensen, S. K. Jespersen, B. Sahl, and E. Falk, "Visual and quantitative evaluation of selected image combination schemes in ultrasound spatial compound scanning," *IEEE Trans. on Medical Imaging* **23**, 181–190, 2004.
19. M. Berson, A. Roncin, and L. Pourcelot, "Compound scanning with an electrically steered beam," *Ultrasonic Imaging* **3**, 303–308, 1981.
20. D. A. Carpenter, M. J. Dadd, and G. Kossoff, "A multimode real time scanner," *Ultrasound Med. and Biol.* **6**, 279–284, 1980.
21. S. Jespersen, J. E. Wilhjelm, and H. Sillesen, "Multi-angle compound imaging," *Ultrasonic Imaging* **20**, 81–102, 1998.
22. G. E. Trahey, S. W. Smith, and O. T. von Ramm, "Speckle patterns correlation with lateral aperture translation: Experimental results and implications for spatial compounding," *IEEE Trans. Ultrason. Ferro. Freq. Contr.* **33**, 257–264, 1986.
23. M. E. Anderson, M. S. Soo, R. C. Bentley, and G. E. Trahey, "The detection of breast microcalcifications with medical ultrasound," *Journal of the Acoustical Society of America* **101**, 29–39, 1997.

24. A. Saleh, S. Ernst, A. Grust, G. Fürst, P. Dall, and U. Mödder, "Real-time compound imaging: Improved visibility of biopsy needles and localization wires as compared to single-line ultrasonography," *Fortschr Röntgenstr* **173**, 368–372, 2001.
25. D. Christensen, *Ultrasonic bioinstrumentation*, John Wiley and Sons, 1988.
26. D. Tran, A. Kamani, V. Lessoway, and R. Rohling, "Adaptive spatial compounding for improving ultrasound images of the epidural space," *proceedings of SPIE* **6513**, 2007.
27. B. Cohen and I. Dinstein, "New maximum likelihood motion estimation schemes for noisy ultrasound images," *Pattern Recognition* **35**, 455–463, 2001.
28. G. P. Penney, J. Weese, J. A. Little, P. Desmedt, D. L. G. Hill, and D. J. Hawkes, "A comparison of similarity measures for use in 2-d–3-d medical image registration," *IEEE Trans. on Medical Imaging* **17**, 586–595, 1998.
29. J. P. W. Pluim, J. B. A. Maintz, and M. A. Viergever, "Mutual-information-based registration of medical images: a survey," *IEEE Transactions on Medical Imaging* **22**, 986–1004, 2003.
30. P. A. Viola and W. M. Wells, "Alignment by maximization of mutual information.," *International Journal of Computer Vision* **24**(2), 137–154, 1997.
31. P. Thévenaz, T. Blu, and M. Unser, "Interpolation revisited," *IEEE Trans. on Med. Imaging* **19**, 739–758, 2000.
32. T. M. Lehmann, C. Gonner, and K. Spitzer, "Survey: interpolation methods in medical image processing," *IEEE Trans. on Med. Imaging* **18**, 1049–1075, 1999.
33. G. Wolberg, *Digital image warping*, IEEE Computer Society Press, 1994.
34. A. Gersho and R. A. Gray, *Vector quantization and signal compression*, Springer-Verlag, 1992.
35. J. Canny, "A computational approach to edge detection," *IEEE Trans. Pattern Analysis and Machine Intelligence* **8**, 679–714, 1986.
36. M. Heath, S. Sarkar, T. Sanocki, and K. Bowyer, "Comparison of edge detectors: a methodology and initial study," *Computer and Image Understanding* **69**, 38–54, 1998.
37. J. Shen and S. Castan, "An optimal linear operator for step edge detection, computer vision," *CVGIP: Graphical Models and Image Processing* **54**, 112–133, 1992.
38. S. Alkaabi and F. Deravi, "Variations of ISEF edge detectors," *Electronics Letters* **39**, 1174–1175, 2003.
39. M. Sharifi, M. Fathy, and M. T. Mahmoudi, "A classified and comparative study of edge detection algorithms," *Proc. of the Int. Conf. on Inf. Tech.: Coding and Computing* , 117–120, 2002.
40. U. Bae and Y. Kim, "Real-time ultrasound elastography," *proceedings of SPIE* **6513**, 2007.